Switching from a Unicellular to Multicellular Organization in an *Aspergillus niger* Hypha

Robert-Jan Bleichrodt,[a,c,d] Marc Hulsman,[b,c,e] Han A. B. Wösten,[a,c] Marcel J. T. Reinders[b,c]

Microbiology, Utrecht University, Utrecht, The Netherlands[a]; Delft Bioinformatics Lab, Intelligent Systems, Department of Electrical Engineering, Mathematics and Computer Science, Delft University of Technology, Delft, The Netherlands[b]; Kluyver Centre for Genomics of Industrial Fermentation, Delft, The Netherlands[c]; Manchester Fungal Infection Group, Institute of Inflammation and Repair, Faculty of Medical and Human Sciences, University of Manchester, Manchester, United Kingdom[d]; Department of Clinical Genetics, VU University Medical Center, Amsterdam, The Netherlands[e]

R.-J.B. and M.H. contributed equally to this article.

ABSTRACT **Pores in fungal septa enable cytoplasmic streaming between hyphae and their compartments. Consequently, the mycelium can be considered unicellular. However, we show here that Woronin bodies close ~50% of the three most apical septa of growing hyphae of *Aspergillus niger*. The incidence of closure of the 9th and 10th septa was even ≥94%. Intercompartmental streaming of photoactivatable green fluorescent protein (PA-GFP) was not observed when the septa were closed, but open septa acted as a barrier, reducing the mobility rate of PA-GFP ~500 times. This mobility rate decreased with increasing septal age and under stress conditions, likely reflecting a regulatory mechanism affecting septal pore diameter. Modeling revealed that such regulation offers effective control of compound concentration between compartments. Modeling also showed that the incidence of septal closure in *A. niger* had an even stronger impact on cytoplasmic continuity. Cytoplasm of hyphal compartments was shown not to be in physical contact when separated by more than 4 septa. Together, data show that apical compartments of growing hyphae behave unicellularly, while older compartments have a multicellular organization.**

IMPORTANCE **The hyphae of higher fungi are compartmentalized by porous septa that enable cytosolic streaming. Therefore, it is believed that the mycelium shares cytoplasm. However, it is shown here that the septa of *Aspergillus niger* are always closed in the oldest part of the hyphae, and therefore, these compartments are physically isolated from each other. In contrast, only part of the septa is closed in the youngest part of the hyphae. Still, compartments in this hyphal part are physically isolated when separated by more than 4 septa. Even open septa act as a barrier for cytoplasmic mixing. The mobility rate through such septa reduces with increasing septal age and under stress conditions. Modeling shows that the septal pore width is set such that its regulation offers maximal control of compound concentration levels within the compartments. Together, we show for the first time that *Aspergillus* hyphae switch from a unicellular to multicellular organization.**

Received 20 January 2015 **Accepted** 28 January 2015 **Published** 3 March 2015

Citation Bleichrodt R, Hulsman M, Wösten HAB, Reinders MJT. 2015. Switching from a unicellular to multicellular organization in an *Aspergillus niger* hypha. mBio 6(2):e00111-15. doi:10.1128/mBio.00111-15.

Invited Editor Reinhard Fischer, Karlsruhe Institute of Technology (KIT), Institute for Applied Biosciences **Editor** B. Gillian Turgeon, Cornell University

Address correspondence to Han A. B. Wösten, h.a.b.wosten@uu.nl, or Marcel J. T. Reinders, m.j.t.reinders@tudelft.nl.

Animals have a multicellular organization. Intercellular cytosolic continuity is restricted by gap junctions that allow streaming of small molecules (≤1,000 Da) such as ions, second messengers, and small metabolites (1). Plasmodesmata mediate intercellular cytosolic continuity in plants. They enable translocation of water, metabolites, proteins, RNA, and viral genomes (2). Plants have been proposed to have a supracellular organization because of their intercellular transport properties (3). Notably, intercellular transport in plants is controlled by changing the pore diameter of plasmodesmata (4–6).

The mycelium of the lower fungi (like the Zygomycota) consists of hyphae that are nonseptate. As a consequence, the mycelium can be considered to be unicellular. The hyphae of higher fungi (those belonging to the Ascomycota and Basidiomycota phyla) are compartmentalized by septa. These septa have a central pore of 50 to 500 nm that allows translocation of water, metabolites, proteins, RNA, and even organelles (7–10). Septa are closed upon hyphal damage to prevent excessive loss of cytoplasm (7, 11–16). They can also be closed in intact growing hyphae (17–19). The septal pore cap mediates septal plugging in the basidiomycete *Schizophyllum commune*. It is a specialized form of the endoplasmic reticulum (ER) that has been proposed to release plugging material into the septal pore (20). In ascomycetes, Woronin bodies plug septal pores. The lumen of these peroxisome-derived organelles (13, 21–23) is filled with hexagonal rods of the HexA protein (13, 24). Deletion of the gene encoding HexA in *Neurospora crassa*, *Magnaporthe grisea*, and *Aspergillus oryzae* results in the absence of Woronin bodies (13–16). As a consequence, hyphal injury results in severe cytoplasmic bleeding (13–16), while heterogeneity in cytosolic composition between neighboring hyphae of *A. oryzae* is severely reduced (19).

Hyphae at the periphery of *Aspergillus* colonies are heterogeneous with respect to cytosolic composition and transcriptional and translational activity (25–32). For instance, only part of the

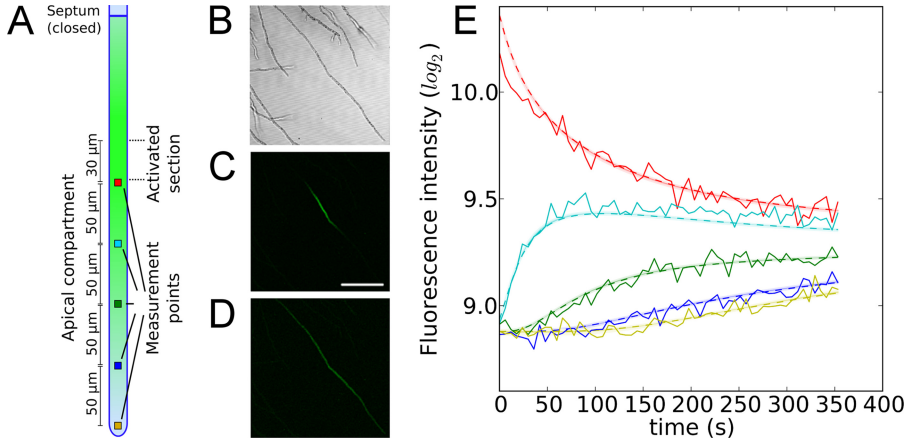

FIG 1 Modeling of PA-GFP streaming assuming random motion of the reporter. (A to C) PA-GFP was activated at $t = 0$ in a closed apical compartment of strain RB#14.5. Bar = 100 μm. (D) After 6 min, PA-GFP had streamed to the apex and subapical regions. (E) Real-time fluorescence intensity profiles were used to model streaming of PA-GFP. The solid and dashed lines indicate real data and model fit, respectively. The color of the line refers to the measurement points in panel A. The standard deviation between model fit and measurements of 5 hyphae was 0.06 in log space.

hyphae highly expresses genes that are involved in substrate degradation (27, 28, 32). Heterogeneity is maintained by septal closure that prevents intercompartmental cytosolic mixing within and between hyphae (19). It was shown that 40% of the apical septa of hyphae at the periphery of *A. oryzae* colonies are closed by Woronin bodies. Closure of the septal pores was reversible and not related to environmental conditions or to the plugging state of neighboring septa. This suggests that septal plugging in *A. oryzae* by Woronin bodies is a stochastic process.

Here, we studied the impact of both open and closed septa on cytosolic continuity in *Aspergillus niger*. The number of septa per hyphal unit, incidence and dynamics of septal closure, and rate of streaming of molecules within the hyphal compartments and through the septal pores was determined and used as input for a model of cytosolic continuity. Our hypothesis was that cytosolic continuity is limited by septal plugging and by the diameter of the open septal pore. It is shown that the mobility of molecules through open septal pores is reduced over time and under stress conditions. Moreover, the incidence of plugging increases as the septa become older. Modeling reveals that in this way young compartments of *A. niger* hyphae switch, over time, from a unicellular to a multicellular organization.

RESULTS

Septal plugging in *A. niger* increases in older compartments. The wild-type *Aspergillus niger* strain N402 was grown on CD medium (19) plus Met for 2 days. The first (apical) compartment of hyphae at the colony periphery or one of the following 9 compartments was dissected using a UV laser. Streaming of cytoplasm from the subapical, neighboring compartment to the damaged compartment was used to score whether septa were open or closed (19) (see Text S1 in the supplemental material). It was found that 57%, 57%, and 52% of the first, second, and third septa were open, respectively (95% confidence interval based on 40 scored septa each, 42% to 72%, 42% to 72%, and 37% to 67%, respectively). In contrast, only 5% (1% to 15%), 8% (2% to 19%), 10% (3% to 22%), 5% (1% to 15%), and 13% (5% to 25%) of the 4th to 8th septa were open, respectively, while the 9th and 10th septum were almost always closed (0% to 6% open septa). Apical septa were almost always open in the Δ*hexA* strain that has no Woronin bodies (33), showing that Woronin bodies are involved in plugging of the apical compartment. Notably, 15% (7% to 28%) of the 9th and 10th septa were still found to be closed in this strain, indicating the existence of another plugging system(s) in these subapical septa.

To determine the dynamics of septal plugging, *A. niger* strain RB#14.5 expressing photoactivatable green fluorescent protein (PA-GFP) from the *gpdA* promoter was grown for 2 days on MM agar with 25 mM maltose (25). PA-GFP was activated by 405-nm laser light within the entire second compartment of hyphae at the periphery of the colony. Hyphae that did not show streaming of PA-GFP to neighboring compartments were selected. Time-lapse movies showed that in 20 out of 52 compartments, PA-GFP started to stream to neighboring compartments within a 16-h period. This showed that plugging of septa in these 20 compartments was released. On average, septa reopened after 4.2 h ± 5.0 h. Thus, septal plugging is reversible in *A. niger*.

Cytosolic mixing of GFP is partially cytoskeleton dependent. *A. niger* strain RB#14.5 was grown as described above. Hyphae in which the first septum was closed were selected. PA-GFP was activated within a 30-μm-wide region 200 μm away from the hyphal tip. Time-lapse movies showed that PA-GFP was streaming in both directions of the apical compartment (Fig. 1). Fluorescence profiles of 5 hyphae were made every 6 s for 5 min. The fluorescence intensity profiles 200, 150, 100, 50, and 0 μm away from the tip were used to model the streaming process. To test whether PA-GFP was streaming by diffusion, we fitted a diffusion model (short-term model [see Fig. S1 in the supplemental material]). The model could be fitted with good accuracy, and we obtained the PA-GFP diffusion rate (Fig. 1E). All diffusion coefficients throughout this study were obtained by model fitting. The deviation between model fit and measurements had an average standard deviation (SD) of 0.06 in log space (for 5 hyphae). This implies that PA-GFP moves by random Brownian-like motion. Bidirectionality of PA-GFP diffusion was also shown by following streaming of the reporter out of a branch of dichotomously branched hyphae. PA-GFP diffused with similar rates in the direction of the tip and in the subapical region of the neighboring branch (Fig. S2).

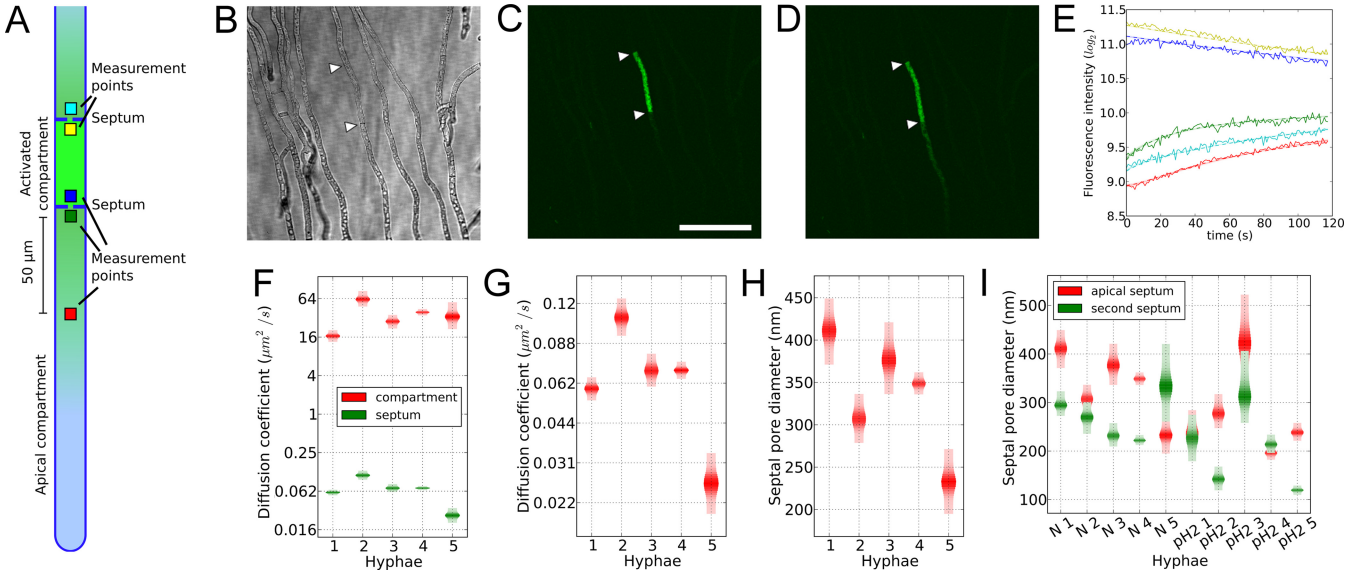

FIG 2 Assessment of the diffusion coefficient of PA-GFP within hyphal compartments and through septal pores. (A to C) PA-GFP was activated in the second compartment of a leading hypha of strain RB#14.5. (D) After 2 min, PA-GFP had streamed to the apical compartment via the first septum. The second septum is closed. Arrowheads point to the septa in panels B to D. Bar = 100 μm. (E) Fluorescence intensity in time at the measurement points indicated in panel A. The dashed lines indicate the model fit based on this data. (F) Diffusion coefficients within the compartment or through the septal pores. (G) Diffusion coefficients of the septal pores in more detail. (H) Septal pore diameters, determined from hyphal diameter and septal and cytosolic diffusion coefficients. (I) Calculated pore diameters of the 1st (red) and 2nd (green) septa under standard conditions (N 1 to N 5) and low-pH conditions (pH2 1 to pH2 5), assuming that the diameter is linearly related to the septal diffusion rate. The uncertainty in these parameter estimates is shown by plotting the distributions for the 95% confidence intervals (F to I).

The diffusion rate of PA-GFP cannot be accurately expressed as a speed, as the fluorescence data are threshold dependent. However, an approximation based on Fig. 2F revealed mobility rates exceeding 5 μm s^{-1}. In contrast, bulk flow of cytosolic particles (of unknown identity) moved with a speed of 0.026 μm s^{-1} ± 0.012 μm s^{-1} toward the tips of hyphae. This matched the growth speed of the hypha (0.023 ± 0.006 μm s^{-1}) and is too slow to impact the short-term (diffusion) model fit. To assess the role of the cytoskeleton in cytosolic mixing of PA-GFP, activation of the reporter was either preceded or not preceded with a 90-min incubation with 1% dimethyl sulfoxide (DMSO), 100 μg ml^{-1} nocodazole (NOC) in 1% DMSO, 80 μg ml^{-1} cytochalasin A (CA) in 1% DMSO, or a cocktail of cytochalasin A and nocodazole (CA-NOC) in 1% DMSO (see Fig. S3A in the supplemental material). NOC and CA cause degradation of the tubulin and actin cytoskeleton, respectively. The short-term model was fitted to measured fluorescence profiles (Fig. S3B to S3F). Only measurements with a high-quality model fit (SD of <0.09) were considered (23 out of 30 measurements). Diffusion coefficients dropped significantly by 22% and 28% when the cultures had been incubated with NOC or CA, respectively, but not when incubated with 1% DMSO alone (Fig. S3G). When the cultures had been incubated with a cocktail of NOC and CA, the diffusion coefficients dropped by 24%. This shows that cytosolic streaming is facilitated by both the actin and tubulin cytoskeleton but also by other unknown forces.

Next, we determined whether diffusion rates could be affected by the plugging state of nearby septa. Therefore, the diffusion coefficients of hyphae with a closed apical septum (Fig. 1) were compared to those in which the two most apical septa were open (as determined by activating PA-GFP in the second compartment [Fig. 2A]). Indeed, intracellular diffusion coefficients of hyphae with open septa were found to be significantly higher (increasing on average from 16 μm^2 s^{-1} to 33 μm^2 s^{-1} [*P* value of 0.013]).

Mobility of PA-GFP through the septal pore. PA-GFP does not stream to a neighboring compartment when the pore is closed (19) (Fig. 2D, top septum). Here it was assessed to which extent open pores affect intercompartmental streaming. To this end, *A. niger* strain RB#14.5 was grown as described above. PA-GFP was activated in the second compartment of leading hyphae (Fig. 2A to D), and 2-min time-lapse movies were made. The short-term model was extended with a septal diffusion coefficient (see Fig. S1B in the supplemental material). This enabled us to study the impact of open pores on cytosolic streaming. Hyphae in which the two most apical septa were open were selected. Measurement points for fluorescence intensity of PA-GFP were set directly before and after the first and second septa and 50 μm from the septal pore in the apical compartment (Fig. 2A). A median diffusion coefficient of 33.3 μm^2 s^{-1} was found within the hyphae (1 SD, 21.6 to 51.2 μm^2 s^{-1}) (Fig. 2F). In contrast, the diffusion coefficient for the first septum was only 0.07 μm^2 s^{-1} (1 SD, 0.04 to 0.11 μm^2 s^{-1}), representing almost a 500-fold difference. This low septal diffusion coefficient can be explained by the diameter of the septal pore. The calculated diameter of septal pores of *A. niger* is on average 335 nm (Fig. 2H), which agrees with the pore sizes that have been experimentally determined in filamentous fungi (7–10).

A simulation was performed to assess the impact of the low septal diffusion coefficient on intercompartmental streaming. In the simulation, a compound was produced in the 2nd compartment at a constant rate for 2 min. A 2-fold difference in concentration of the compound was found in this compartment after 2 min of production in the presence of septa compared to their

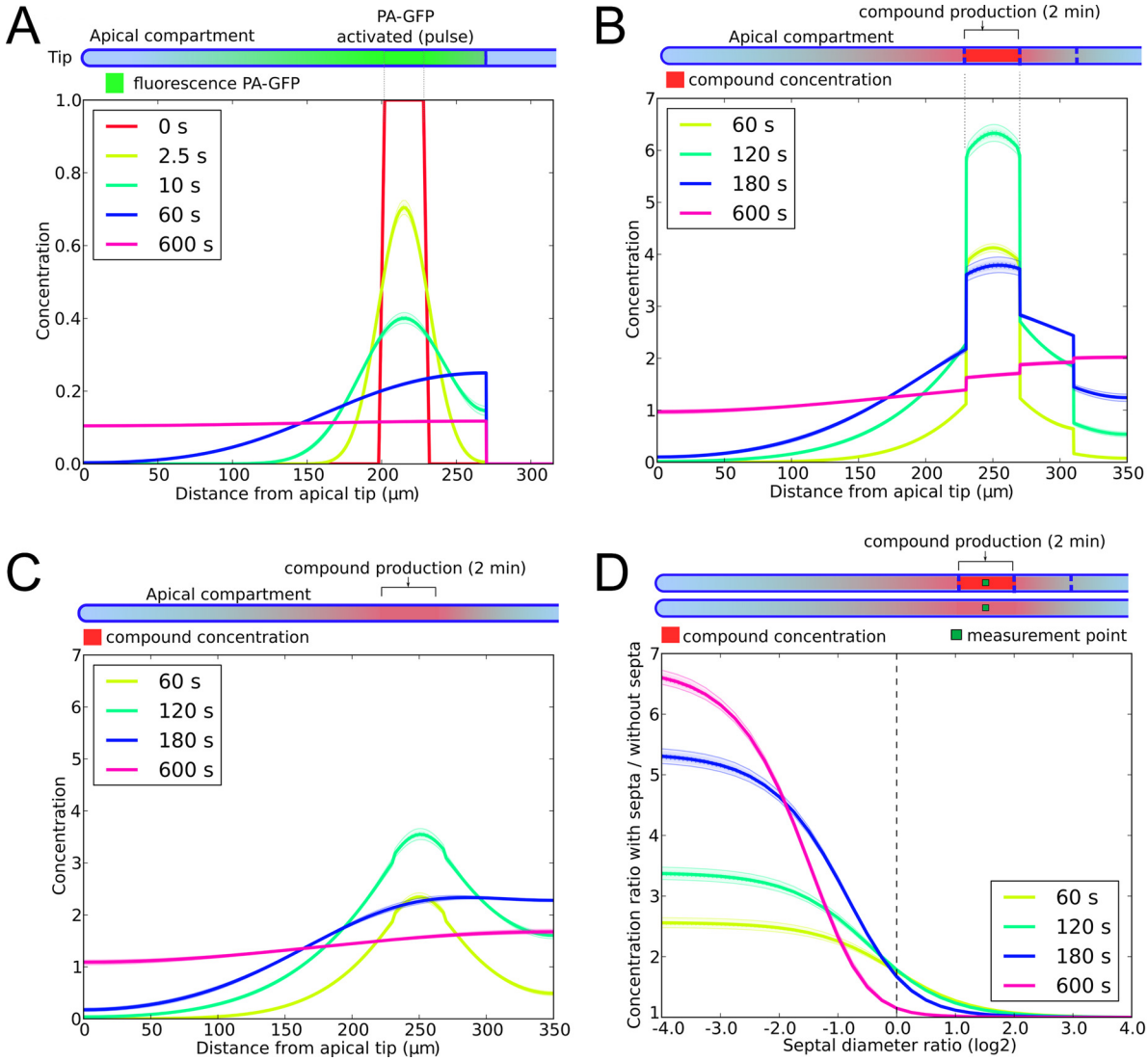

FIG 3 Simulation of PA-GFP diffusion rate in a hypha. (A) PA-GFP was activated at $t = 0$ in the region 200 to 230 μm away from the tip. The apical septum is closed. Diffusion coefficients were obtained by fitting experimental data (Fig. 2F). (B) Influence of open septa on concentration of compounds. A compound is produced for 2 min at a constant rate in the 2nd compartment and is allowed to diffuse. (C) The concentration of the compound can reach levels up to 2-fold higher in the first compartment than those in the second compartment due to the presence of an open septum compared to a situation without a septum. (D) Simulation of the effect of changing the septal pore diameter. The concentration ratio observed between an activated compartment (with open septa, as in panel B) and an activated region (without septa, as in panel C) after producing a certain compound for 2 min at a constant rate is plotted. Septal pores with widths as observed in Fig. 2H (on average, 335 nm) were used as the reference ($\log_2$ ratio = 0; indicated by the vertical dashed line).

absence (Fig. 3). This difference in concentration, which did not depend on the production rate, had disappeared 8 min after production had stopped. Together, open septa form a barrier for intercompartmental streaming of compounds on a time scale of minutes.

Relatively large differences were observed between septal diffusion coefficients (ranging from 0.03 to 0.11 $\mu m^2\ s^{-1}$ [Fig. 2G]). These differences could be explained either by differences in the cytosolic diffusion rate (also affecting the diffusion rate within the pore) or by differences in the septal pore diameter. Only a limited correlation between the cytosolic diffusion parameters and the septal diffusion parameters was observed (Fig. 2F), suggesting that the septal pore diameter plays an important role. The differences in septal pore diameter (with an average of 335 nm ± 62 nm) exceeded estimation uncertainty (Fig. 2H), indicating that septal pores indeed vary in width. Subsequently, we elaborated how the septal pore diameter would affect the concentration of a compound in the producing compartment assuming that the rate of diffusion through the septal pore is linearly dependent on its cross-sectional area (note that diffusion rates will be lower close to septal pore walls). Simulations revealed that changing the diameter of the septal pore has relatively large effects (Fig. 3D). For instance, almost no differences in concentration in the 2nd compartment were observed after 10 min between a simulation with and without septa with a pore of 335 nm assuming a production of a compound for 2 min in the 2nd compartment (ratio of 1.1 for a $\log_2$ ratio of 0 in Fig. 3D). However, reducing the septal pore diameter to 25% of its size (from 335 to 84 nm; $\log_2$ ratio of −2 in

Fig. 3D) increased this ratio to 4.8. The 50- to 500-nm septal pore diameter range reported (7–10) conforms to a $\log_2$ range of −2.7 to 0.6, which covers the range that offers the largest effect on concentrations (Fig. 3D, the $\log_2$ range of −2.7 to 0.6 on the *x* axis corresponds to the steepest sections of the concentration ratio curves). In comparison, the 5 hyphae (Fig. 2H) that were measured under the same conditions were observed to cover a $\log_2$ diameter range of −0.5 to 0.3 (corresponding to diameters of 232 to 411 nm).

Septal pore plugging is not affected by low pH (33). Here we assessed whether this environmental condition impacts the diffusion rate within the septal pore. The diffusion rates of the first and second septa were determined for hyphae grown under standard growth conditions (see above) and for hyphae that had been exposed to pH 2 for 1.5 h. Under both growth conditions, the diffusion rate was higher in the first septum than in the second septum. Data suggest that the diameter of the second pore is reduced 22% (which equals a reduction of 68 nm in diameter) compared to that of the first septum. Data also showed that the septal pore diffusion coefficients ($\mu m^2\ s^{-1}$) of the first and second septa were significantly lower under low-pH conditions (on average, 0.061 versus 0.034 and 0.040 versus 0.018, respectively [$n = 5$] [SD of mean, 0.012, 0.002, 0.010, and 0.006, respectively]). These data suggest that low pH induces the septal pore to narrow by 21% (equals a reduction of 64 nm in diameter) (Fig. 2I).

Next, whether diffusion rates were similar through apical septa that had never been closed and septa that had reopened was examined. To this end, PA-GFP was activated in the second hyphal compartment. Time-lapse movies of 16 h were produced with an image taken every 15 min. Compartments that showed septa opening within this period were selected. The model was fitted to obtain the diffusion rates of PA-GFP. The pore widths of 2 out of 3 reopened septa were smaller (143 and 207 nm) (see Fig. S4F in the supplemental material) than those of septa that had never been closed (232 to 411 nm) (Fig. 2H). Notably, the longer the septal pore had been closed, the lower the calculated pore width was (Fig. S4E and S4F). This indicates that septa do not completely reopen after septal plugging. It was also observed that reopened septa could plug again as indicated by the disequilibrium of hypha 2 and 3 (Fig. S4C and S4D). This further substantiates the concept of reversible septal plugging.

Factors that influence hyphal heterogeneity. The long-term simulation model was used to determine which factors influence heterogeneity between the apical sections of a dichotomously branched hypha at longer time scales (multiple hours) (Fig. 4A). To this end, the short-term model was extended with processes that affect cytosolic streaming at these time scales (hyphal extension, protein production/degradation, formation of septa, and plugging dynamics; see Fig. S5A in the supplemental material). Parameterization was based on a hyphal growth rate of 137 ± 13 $\mu m\ h^{-1}$, an apical compartment length of 279 ± 114 μm, and an average subapical compartment length of 45 ± 19 μm. Diffusion coefficients were sampled from the experiment shown in Fig. 2F. The compound degradation half-life and septal plugging rate were varied to determine the extent of their effect. The concentration of a compound was set at 1.0 in one of the two apical compartments at a given distance between the tips of the hyphae. The concentration profile of the compound at the tip of the other hypha was determined over time through simulation (Fig. 4B). Diffusion effectively mixed the cytoplasm of the two hyphae in the absence of septa (Fig. 4G). The effectiveness of mixing decreased only gradually when the distance between the tips increased due to growth. Introducing the presence of open septa in the simulation reduced cytosolic mixing efficiency (as indicated by the maximum concentration reached) by 2- to 3-fold (Fig. 4F). Mixing became ineffective when there were more than 4 septa that switched between the open and closed states (Fig. 4E). As was found for short time scales, a reduction in diameter of the septal pore had a significant impact on diffusion, even when only 1 septum separated the apical compartments (Fig. 4H). Reducing the diameter of the septal pore 2-fold (from 335 to 168 nm) reduced the maximum concentration reached in the nonactivated apical compartment by approximately 2.

The average septal plugging switch time [$(\lambda_{open} + \lambda_{closed})/2$] and degradation time were both set at 1 h for the experiments described in the previous sections. Changing these values had limited effect on the concentration peaks at the apical tip (Fig. 4D). For example, changing the septal plugging switch time from 1 to 2 h only slightly reduced the average maximum concentration from 0.25 to 0.22. The limited impact of the degradation rate can be explained by the dilution taking place due to hyphal extension. At a 137 $\mu m\ h^{-1}$ growth rate (see above), concentrations in closed apical compartments already have a half-life of approximately 2 h without any additional degradation occurring.

Three scenarios for emergence of heterogeneity between two neighboring hyphae were tested. In the first scenario, a regulator is switched on in one hypha at the moment that branching between the two hyphae has occurred. In the second and third scenario, the regulator is either activated or inhibited in one of the hyphae after a total of 2 septa have separated the two neighboring apices. Production of the regulator when activated was simulated to take place at a rate of the base production rate multiplied by (1.0 − current concentration min^{-1}) using a degradation half-life of 1 h and a base production rate of 0.1. It was found that activation of a gene after separation by two septa was the most effective way to obtain the largest concentration differences between two apical neighboring tips (Fig. 4C). This conclusion also holds for a production rate that is 10 times slower or a degradation half-life of 10 min, although in this case delaying the activation of the regulator provides only a small benefit.

The model showed that (reversible) septal plugging has a major impact on intercompartmental cytosolic streaming. Therefore, it was tested to which extent septal plugging prevents cytosolic streaming *in vivo*. Transformants RB#200.4, RB#200.6, and RB#200.7 expressing H2B-GFP (H2B stands for histone 2B) (nuclear localization) and dTomato (freely diffusible) under control of the inducible *glaA* promoter were grown on MM agar medium with 200 mM xylose (*glaA* repressing) or 25 mM maltose (*glaA* inducing). After 5 days, the colonies were transferred to 25 mM maltose for 6 h. The fluorescence intensity of hyphae at the outer part of the colony was measured (see Fig. S6M to S6P in the supplemental material). All transformants showed heterogeneous fluorescence intensities of H2B-GFP and dTomato after 6-h induction (Fig. S6A to S6L and Table S1). This indicates that cytosolic streaming is limited. After 5-day induction, 2 out of 3 transformants still showed heterogeneity. This shows that cytosolic streaming still has limited effect on reducing heterogeneity on longer time scales. To test the extent of cytosolic streaming, Spearman correlation coefficients were calculated between nuclear H2B-GFP and cytosolic dTomato fluorescence intensity within

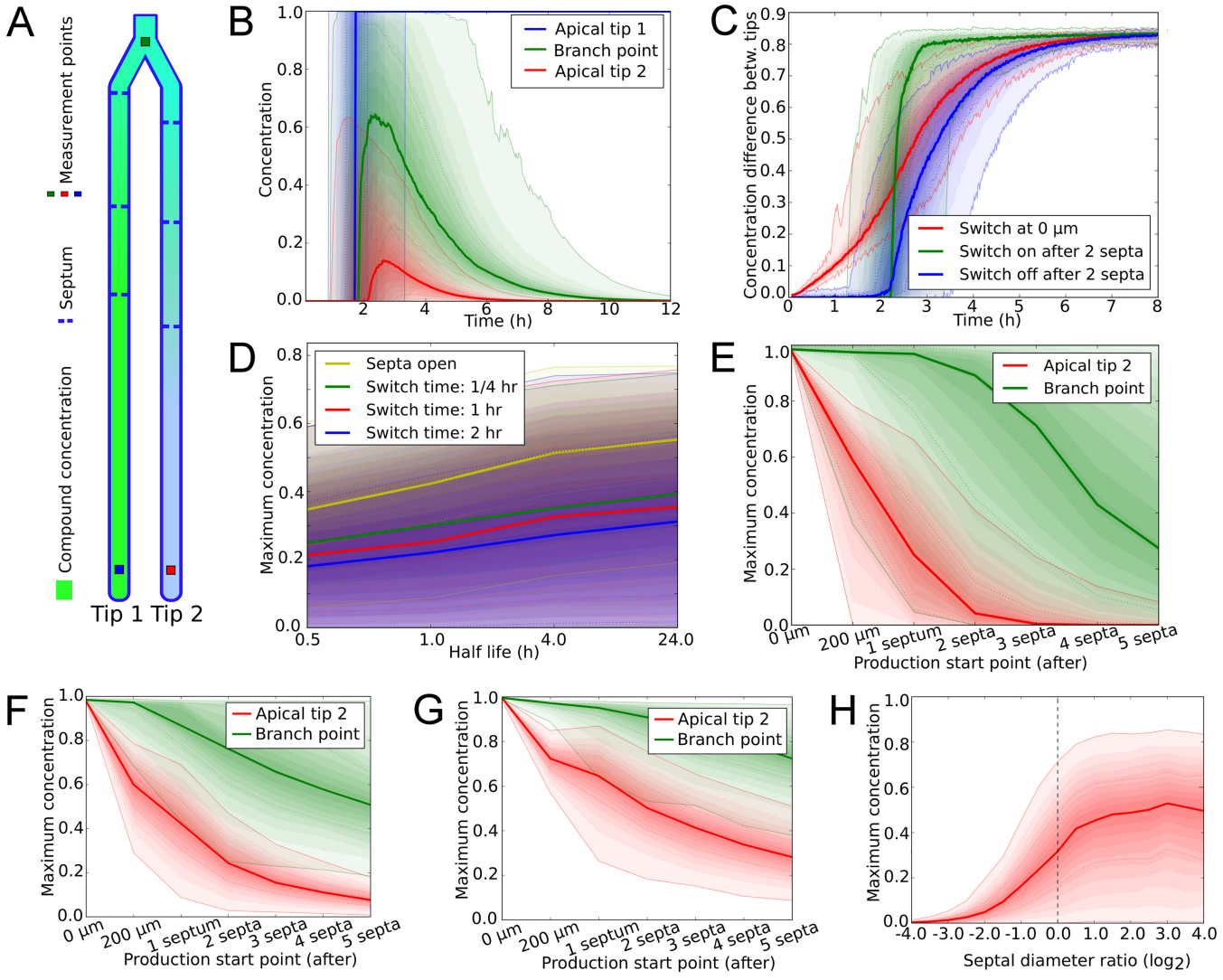

FIG 4 Long-term simulation of compound concentration in a branched hypha. (A) The compound concentration was measured in hyphal tips and branch points. (B) The compound concentration in apical compartment 1 is set at 1 at $t = 0$. In hyphal tip 2, the maximum concentration level reached by diffusion is not maintained, but decreases quickly due to growth, degradation, and septum formation. (C) Scenarios of the emergence of heterogeneity. A switch in the regulatory program at the branch (one branch turns a gene on) compared to a delayed switch, either turning the gene off or on in one branch. The differences in compound concentrations between the tips is shown. (D) Effects of half-life and septal plugging switch time on the maximum concentration reached in apical tip 2. (E) Cytosolic continuity between branches at different growth stages. Production in hyphal tip 1 after a certain branch length/number of septa have been formed. (F and G) Same experiment as in panel E but with open septa or without septa, respectively. (H) Effect of septal pore diameter on cytosolic continuity. Apical compartment 1 is activated. The maximum compound concentration in hyphal tip 2 is shown. In panels B to H, the lines and shaded areas indicate the median values and the ranges of the values (95% confidence interval), respectively. Expression changes/starts after 2 septa (B to D) or 1 septum (H) have formed.

individual hyphae. The correlation was 0.71 ± 0.12 in the case of the 6-h induction, while it was significantly lower (0.46 ± 0.08) in the case of 5-day induction. This shows that reversible septal plugging maintains heterogeneity, but also allows cytosolic streaming between neighboring hyphae on long time scales (5 days) when they are separated by less than 4 septa.

DISCUSSION

A fungal mycelium consists of hyphae that grow at their tips and that branch subapically. Zones within a mycelium show heterogeneity in gene expression, growth, and secretion (25, 26, 30, 31, 34–39). For instance, 9% of the active genes in colonies of *A. niger* are expressed in only one out of five concentric zones, while 25% of the active genes show at least a 2-fold difference in expression between the outer and innermost zone of the colony (35). Even hyphae within a zone of a mycelium are heterogeneous with respect to cytosolic composition (19, 25–32, 40). For instance, only part of the hyphae at the periphery of a mycelium of *A. niger* highly expresses the glucoamylase gene *glaA* (27). Hyphal heterogeneity in the mycelium is in conflict with the concept of cytosolic continuity that would result from cytosolic mixing due to intercompartmental streaming within and between hyphae enabled by the presence of septal pores. However, we recently showed that part of the apical septa of growing vegetative hyphae of *A. oryzae* is closed (19). Plugging of apical septa was no longer observed in a Δ*hexA* strain that does not contain Woronin bodies. As a consequence,

hyphal heterogeneity was strongly reduced. Here, we elaborated on this study assessing the impact of both open and closed septa on intercompartmental cytosolic streaming. It is shown that the youngest part of a growing hypha can be considered unicellular, while the older part has a multicellular organization. A unicellular organization may support growth of rapidly growing leading hyphae. On the other hand, a multicellular organization may reduce invasion of noncompatible partners and pathogens such as viruses. In addition, multicellularity maintains heterogeneity between hyphae and compartments, and this may increase survival in a dynamic environment.

Cytosolic streaming can be described as a diffusion process with a speed that exceeds 5 μm s^{-1}. Particles in the hyphae (of unknown identity) moved with approximately 200-fold-lower speed. This bulk flow was similar to the growth speed of the hyphae and should therefore be sufficient to support apical growth. However, the bulk flow was too slow to impact the short-term (diffusion) model fit. In contrast, bulk flow does impact intercellular transport in *N. crassa*. The driving force behind this bulk flow is the osmotically regulated emergence of pressure gradients (41). The bulk flow is directed to the tip and can reach velocities as high as 60 μm s^{-1} (10). The cytoskeleton also has a role in transport in *N. crassa* by for instance providing retrograde and accelerated anterograde movement of nuclei (42). The addition of cytochalasin A and nocodazole was used to assess the roles of actin and tubulin, respectively, on cytosolic streaming in *A. niger*. Both drugs or their combination reduced cytosolic streaming rates by about 25%. The impact of the cytoskeleton on cytosolic streaming can be explained by turbulence created by bidirectional movement of molecular motors and their cargo along the cytoskeleton (43). The fact that this turbulence would account for 25% of the streaming implies the roles of other mechanisms such as turgor pressure (10).

About 60% of the three most apical septa of growing vegetative hyphae of *A. oryzae* are open (19). This is similar to the closure incidence of ~50% in the case of *A. niger*. The presence of a branch near the septum did not correlate with increased plugging (data not shown). Notably, only about 10% of the septa of the 4th to 8th compartment were open in *A. niger*, while those of the 9th and 10th compartment were almost always closed. The closure of septa is reversible in the case of the apical septa, but in the case of the 9th and 10th septa, this is not expected to be the case. Since 40 septa were measured, there is still a small chance (up to 6%) that septa of the 10th compartment occasionally reopen. This is due to the fact that septa showed a reopening time of about 4.2 h. In this time, the 2nd compartment will become at least a 10th compartment due to hyphal growth.

Modeling showed that an open septum is a short-term barrier for intercompartmental mixing of the cytoplasm. The diffusion through septal pores was shown to be 500 times lower than that within the hypha. This difference can be explained by the ratio of the cross-sectional area of the septal pore compared to that of the hypha. Based on electron microscopy images (16, 44; our data), it can be calculated that the difference in cross-sectional area of a septal pore compared to that of the hypha matches the difference in the fold change in diffusion. The lower diffusion coefficient within the septal pore can maintain heterogeneity on a time scale of minutes. Interestingly, the diffusion coefficient was different between septa, with consistent changes being observed between apical and nonapical septa (22%), with septa under low-pH conditions (21%), and septa that had reopened after a period of closure. It may well be that these differences in diffusion coefficients are due to differences in the diameter of the septal pore. Septal pore sizes of 50 to 500 nm have been reported in filamentous fungi (7–10). This closely matches the results of our model that implied an average diameter of 335 nm ± 62 nm. Interestingly, this diameter is in the range where changes have the largest effects on compartment concentrations. It is tempting to speculate that dynamic adjustment of the septal pore diameter is a way to regulate intercompartmental mixing of the cytoplasm to reduce or increase heterogeneity between hyphal compartments. The extent and functional identity of hyphal compartments are not yet known and will be studied in the near future with single-compartment transcriptomics (30).

The variation in diameter of the septal pore may be explained by septal pore-associated proteins (SPAs). These proteins accommodate variation in septal pore diameter in *N. crassa* by forming aggregates (45). SPA-like proteins have also been found in *Aspergillus nidulans* (46). Aggregates of SPA-like proteins may be involved in permanent closure of the septa in the 9th and 10th compartments. These aggregates may do so by interacting with Woronin bodies or simply by forming a plug by themselves. Interaction with the Woronin body is suggested by the finding that a longer period of plugging correlated with a lower predicted pore width. A mechanism independent of Woronin bodies is suggested from the finding that 15% of 9th and 10th septa were still closed in a Δ*hexA* strain of *A. niger* that does not form Woronin bodies. It should be noted that organelles like vacuoles regularly are found near the septal pore. These vacuoles can temporarily block the septal pores and therefore are an additional factor impacting streaming through the septa.

Modeling showed that the incidence of septal plugging (57%, 57%, 52%, and 5% for the first 4 septa) impacted heterogeneity on a time scale of hours. In fact, the incidence of septal closure in *A. niger* makes that cytosolic continuity is restricted to a maximum of four apical compartments. Septal plugging thus profoundly impacts cytosolic continuity of the *A. niger* mycelium. It implies that bulk flow of cytoplasm from the center to the periphery of the colony (or vice versa) is nonexistent in the case of *A. niger*. This explains why zones can be heterogeneous in protein and RNA composition (35, 38). Modeling showed that increasing half-life of RNA and/or proteins had limited effect on this cytosolic continuity, as dilution due to hyphal extension was just as effective in reducing the concentrations. On the other hand, simulations showed that hyphal heterogeneity is built up most effectively by activating a gene (rather than gene inhibition) and after branches had formed septa (rather than gene activation in the absence of septa).

The 500-fold difference in diffusion coefficients between septal pores and hyphal compartments is likely explained by the difference in their cross-sectional areas. The diffusion rates within a gap junction are on average 0.005 μm^2 s^{-1} (47), which is more than 6,600 times lower than that of septal pores of *A. niger*. This may also be explained, at least in part, by the cross-sectional area, because pores in gap junctions are considerably smaller than those of fungal septa (diameters of 2 to 3 nm [48] versus 50 to 500 nm [7–10]). In this respect, plasmodesmata with a diameter of 20 to 50 nm (49) would have an intermediate diffusion coefficient. Notably, intercellular transport in plants is controlled by changing the pore diameter of plasmodesmata (3–5). Our data indicate that

fungi also regulate intercellular connectivity by changing the septal pore diameter. This provides a way to reduce or increase heterogeneity, the latter being important for developmental processes and possibly also to survive changing environmental conditions.

MATERIALS AND METHODS

Strains, growth conditions, and analysis of plugging. Strains used in this study, growth conditions, and analysis of plugging are described in Text S1 in the supplemental material.

Reporter studies and analysis of cytosolic bulk flow and hyphal extension. Photoactivatable green fluorescent protein (PA-GFP) activation, fluorescence microscopy, correlation between fluorescence intensity of reporters, and analyses of cytosolic bulk flow and hyphal extension are described in Text S1 in the supplemental material.

Modeling. (i) Modeling cytosolic streaming. PA-GFP was used to monitor streaming of cytosol. Streaming experiments (Fig. 1A) were recreated *in silico* assuming that the observed streaming is the result of cytosolic mixing. The mixing process was modeled as a diffusion process (see Fig. S1B in the supplemental material). Hypha represent a quasi-one-dimensional (quasi-1D) environment, as the width of hypha is negligible compared to their length. Transverse transport due to diffusion is therefore very fast compared to longitudinal transport. Based on this, a constant gradient along the transverse axis can be assumed, allowing a simplification of the model to 1D (along the hyphal length axis), with the diffusion represented by the equation $\frac{\partial f}{\partial t} - D\frac{\partial^2 f}{\partial x^2} = 0$. Here, f represents fluorescence, t is time, x is the position in the hypha, and D is the diffusion coefficient. Hyphae were divided into a grid with a resolution of $\partial x = 2$ μm. Note that the diameter of the hypha does not affect the estimate of the cytoplasmic diffusion coefficient D. Septa were modeled with grid points that were $\partial x_{septa} = 0.25$ μm apart, with the diffusion coefficient between these grid points set to the value D_{septa}. Closed septa were assigned a value of $D_{septa} = 0$. Each grid point in the simulation had 2 neighboring grid points, except for the border (i.e., at the tip) and branching points, which had 1 and 3 neighboring points, respectively. The simulation time step ∂t was set to $0.5\frac{\delta x^2}{2D}$.

Septal locations and compartment sizes were determined experimentally or by an indirect fit based on fluorescence diffusion observations (see parameter estimation below). Simulated fluorescence signal profiles at locations between grid points were obtained through linear interpolation.

(ii) Short-term model. The short-term model was based on parameters (see Data Set S1 in the supplemental material) describing the diffusion coefficients D and D_{septa}, the hyphal compartment lengths, septal plugging state, the initial fluorescence pulse intensity, and the background fluorescence intensity. Unmeasured parameters (e.g., compartment size when apical compartments were longer than the field of view) were estimated using experimental data, by encapsulating the short-term model in a Bayesian model (Fig. S1C). This allowed us to determine the posterior distributions of the diffusion coefficients. Fluorescence signals were assumed to be normally distributed with the variance being distributed according to an inverse gamma prior (the conjugate prior of a normal distribution with known μ) with parameters $\alpha = 1$ and $\beta = 1$. The septal state was modeled using a Bernoulli distribution with probability $P = 5$. Compartment sizes were modeled using a uniform distribution when they had not been experimentally determined (e.g., due to being outside the image frame).

Diffusion coefficients D and D_{septa} were modeled using a log uniform distribution, with limits of 2^0 to 2^8 for the cytoplasm and 2^{-10} to 2^6 for septa. These limits prevented the Bayesian sampling process from sampling unreasonably high diffusion rates that would lead to infeasibly large simulation times due to the associated reduction in the time step ∂t. The initial pulse intensity could not be directly measured due to limitations of the microscope that induced a measurement delay of ~12 s after the initial pulse. The pulse intensity was therefore modeled using a log uniform distribution with as the initial starting estimate a value obtained by extrapolating from the first 5 time points measured in the activated compartment. The background fluorescence intensity was modeled similarly, with initial estimates obtained from measurement points that were not yet affected by the activated PA-GFP.

To estimate the posterior distributions of the parameters, Markov chain Monte Carlo (MCMC) sampling was used by taking at least 250,000 samples with a burn-in of 100,000 samples and a thinning factor of 10.

(iii) Estimation of septal diameter. On the basis of the observation that the differences in the septal diffusion coefficient D_{septa} and the cytosolic diffusion coefficient D could be explained by the difference between hyphal and septal diameter, we estimated the septal pore diameter from our measurements using the following equation: $\text{septal pore diameter} = \sqrt{\frac{D_{septa} * \text{hyphal diameter}^2}{D}}$.

This was done within the Bayesian framework to account for uncertainty in the diffusion coefficients.

(iv) Long-term model. The long-term model was based on the short-term model extended with simulation procedures for hyphal extension, compound production, and degradation, as well as septum formation and dynamic septal plugging, in order to model long-term behavior of the hypha across multiple hours (see Fig. S5 in the supplemental material). This is described in more detail in Text S1.

SUPPLEMENTAL MATERIAL

Supplemental material for this article may be found at http://mbio.asm.org/lookup/suppl/doi:10.1128/mBio.00111-15/-/DCSupplemental.

Text S1, DOCX file, 0.02 MB.
Data set S1, PDF file, 0.1 MB.
Figure S1, TIF file, 2.5 MB.
Figure S2, TIF file, 1.4 MB.
Figure S3, TIF file, 2.4 MB.
Figure S4, TIF file, 0.7 MB.
Figure S5, TIF file, 2.4 MB.
Figure S6, TIF file, 1.8 MB.
Table S1, PDF file, 0.1 MB.

ACKNOWLEDGMENT

This work was supported by The Netherlands Genomics Initiative through a grant of The Netherlands Consortium for Systems Biology.

REFERENCES

1. **Meşe G, Richard G, White TW**. 2007. Gap junctions: basic structure and function. J Invest Dermatol **127:**2516–2524. http://dx.doi.org/10.1038/sj.jid.5700770.
2. **Heinlein M, Epel BL**. 2004. Macromolecular transport and signaling through plasmodesmata. Int Rev Cytol **235:**93–164. http://dx.doi.org/10.1016/S0074-7696(04)35003-5.
3. **Lucas WJ, Lee JY**. 2004. Plasmodesmata as a supracellular control network in plants. Nat Rev Mol Cell Biol **5:**712–726. http://dx.doi.org/10.1038/nrm1470.
4. **Xu XM, Jackson D**. 2010. Lights at the end of the tunnel: new views of plasmodesmal structure and function. Curr Opin Plant Biol **13:**684–692. http://dx.doi.org/10.1016/j.pbi.2010.09.003.
5. **Lee JY, Lu H**. 2011. Plasmodesmata: the battleground against intruders. Trends Plant Sci **16:**201–210. http://dx.doi.org/10.1016/j.tplants.2011.01.004.
6. **Maule AJ, Benitez-Alfonso Y, Faulkner C**. 2011. Plasmodesmata – membrane tunnels with attitude. Curr Opin Plant Biol **14:**683–690. http://dx.doi.org/10.1016/j.pbi.2011.07.007.
7. **Shatkin AJ, Tatum EL**. 1959. Electron microscopy of *Neurospora crassa* mycelia. J Biophys Biochem Cytol **6:**423–426. http://dx.doi.org/10.1083/jcb.6.3.423.
8. **Moore RT, McAlear JH**. 1962. Fine structures of mycota. Observations on septa of ascomycetes and basidiomycetes. Am J Bot **49:**86–94. http://dx.doi.org/10.2307/2439393.

9. **Gull K**. 1978. Form and function of septa in filamentous fungi. The filamentous fungi III, p 7886–93. In Smith JE, Berry DR (ed), Developmental mycology. Wiley, New York, NY.
10. **Lew RR**. 2005. Mass flow and pressure-driven hyphal extension in *Neurospora crassa*. Microbiology **151:**2685–2692. http://dx.doi.org/10.1099/mic.0.27947-0.
11. **Trinci AP, Collinge AJ**. 1974. Occlusion of the septal pores of damaged hyphae of *Neurospora crassa* by hexagonal crystals. Protoplasma **80:**57–67. http://dx.doi.org/10.1007/BF01666351.
12. **Collinge AJ, Markham P**. 1985. Woronin bodies rapidly plug septal pores of severed *Penicillium chrysogenum* hyphae. Exp Mycol **9:**80–85. http://dx.doi.org/10.1016/0147-5975(85)90051-9.
13. **Jedd G, Chua NH**. 2000. A new self-assembled peroxisomal vesicle required for efficient resealing of the plasma membrane. Nat Cell Biol **2:**226–231. http://dx.doi.org/10.1038/35008652.
14. **Tenney K, Hunt I, Sweigard J, Pounder JI, McClain C, Bowman EJ, Bowman BJ**. 2000. *hex-1*, a gene unique to filamentous fungi, encodes the major protein of the Woronin body and functions as a plug for septal pores. Fungal Genet Biol **31:**205–217. http://dx.doi.org/10.1006/fgbi.2000.1230.
15. **Soundararajan S, Jedd G, Li X, Ramos-Pamploña M, Chua NH, Naqvi NI**. 2004. Woronin body function in *Magnaporthe grisea* is essential for efficient pathogenesis and for survival during nitrogen starvation stress. Plant Cell **16:**1564–1574. http://dx.doi.org/10.1105/tpc.020677.
16. **Maruyama J, Juvvadi PR, Ishi K, Kitamoto K**. 2005. Three-dimensional image analysis of plugging at the septal pore by Woronin body during hypotonic shock inducing hyphal tip bursting in the filamentous fungus *Aspergillus oryzae*. Biochem Biophys Res Commun **331:**1081–1088. http://dx.doi.org/10.1016/j.bbrc.2005.03.233.
17. **van Peer AF, Müller WH, Boekhout T, Lugones LG, Wösten HAB**. 2009. Cytoplasmic continuity revisited: closure of septa of the filamentous fungus *Schizophyllum commune* in response to environmental conditions. PLoS One **4:**e5977. http://dx.doi.org/10.1371/journal.pone.0005977.
18. **van Peer AF, Wang F, van Driel KG, de Jong JF, van Donselaar EG, Müller WH, Boekhout T, Lugones LG, Wösten HAB**. 2010. The septal pore cap is an organelle that functions in vegetative growth and mushroom formation of the wood-rot fungus *Schizophyllum commune*. Environ Microbiol **12:**833–844. http://dx.doi.org/10.1111/j.1462-2920.2009.02122.x.
19. **Bleichrodt RJ, van Veluw GJ, Recter B, Maruyama J, Kitamoto K, Wösten HA**. 2012. Hyphal heterogeneity in *Aspergillus oryzae* is the result of dynamic closure of septa by Woronin bodies. Mol Microbiol **86:**1334–1344. http://dx.doi.org/10.1111/mmi.12077.
20. **van Driel KG, van Peer AF, Grijpstra J, Wösten HA, Verkleij AJ, Müller WH, Boekhout T**. 2008. Septal pore cap protein SPC18, isolated from the basidiomycetous fungus *Rhizoctonia solani*, also resides in pore plugs. Eukaryot Cell **7:**1865–1873. http://dx.doi.org/10.1128/EC.00125-08.
21. **Liu F, Ng SK, Lu Y, Low W, Lai J, Jedd G**. 2008. Making two organelles from one: Woronin body biogenesis by peroxisomal protein sorting. J Cell Biol **180:**325–339. http://dx.doi.org/10.1083/jcb.200705049.
22. **Escaño CS, Juvvadi PR, Jin FJ, Takahashi T, Koyama Y, Yamashita S, Maruyama J, Kitamoto K**. 2009. Disruption of the *Aopex11-1* gene involved in peroxisome proliferation leads to impaired Woronin body formation in *Aspergillus oryzae*. Eukaryot Cell **8:**296–305. http://dx.doi.org/10.1128/EC.00197-08.
23. **Managadze D, Würtz C, Sichting M, Niehaus G, Veenhuis M, Rottensteiner H**. 2007. The peroxin PEX14 of *Neurospora crassa* is essential for the biogenesis of both glyoxysomes and Woronin bodies. Traffic **8:**687–701. http://dx.doi.org/10.1111/j.1600-0854.2007.00560.x.
24. **Managadze D, Würtz C, Wiese S, Meyer HE, Niehaus G, Erdmann R, Warscheid B, Rottensteiner H**. 2010. A proteomic approach towards the identification of the matrix protein content of the two types of microbodies in *Neurospora crassa*. Proteomics **10:**3222–3234. http://dx.doi.org/10.1002/pmic.201000095.
25. **Wösten HAB, Moukha SM, Sietsma JH, Wessels JG**. 1991. Localization of growth and secretion of proteins in *Aspergillus niger*. J Gen Microbiol **137:**2017–2023. http://dx.doi.org/10.1099/00221287-137-8-2017.
26. **Wösten HA, van Veluw GJ, de Bekker C, Krijgsheld P**. 2013. Heterogeneity in the mycelium: implications for the use of fungi as cell factories. Biotechnol Lett **35:**1155–1164. http://dx.doi.org/10.1007/s10529-013-1210-x.
27. **Vinck A, Terlou M, Pestman WR, Martens EP, Ram AF, van den Hondel CAMJJ, Wösten HAB**. 2005. Hyphal differentiation in the exploring mycelium of *Aspergillus niger*. Mol Microbiol **58:**693–699. http://dx.doi.org/10.1111/j.1365-2958.2005.04869.x.
28. **Vinck A, de Bekker C, Ossin A, Ohm RA, de Vries RP, Wösten HAB**. 2011. Heterogenic expression of genes encoding secreted proteins at the periphery of *Aspergillus niger* colonies. Environ Microbiol **13:**216–225. http://dx.doi.org/10.1111/j.1462-2920.2010.02322.x.
29. **Etxebeste O, Herrero-García E, Araújo-Bazán L, Rodríguez-Urra AB, Garzia A, Ugalde U, Espeso EA**. 2009. The bZIP-type transcription factor FlbB regulates distinct morphogenetic stages of colony formation in *Aspergillus nidulans*. Mol Microbiol **73:**775–789. http://dx.doi.org/10.1111/j.1365-2958.2009.06804.x.
30. **de Bekker C, Bruning O, Jonker MJ, Breit TM, Wösten HA**. 2011. Single cell transcriptomics of neighboring hyphae of *Aspergillus niger*. Genome Biol **12:**R71. http://dx.doi.org/10.1186/gb-2011-12-8-r71.
31. **de Bekker C, van Veluw GJ, Vinck A, Wiebenga LA, Wösten HA**. 2011. Heterogeneity of *Aspergillus niger* microcolonies in liquid shaken cultures. Appl Environ Microbiol **77:**1263–1267. http://dx.doi.org/10.1128/AEM.02134-10.
32. **van Veluw GJ, Teertstra WR, de Bekker C, Vinck A, van Beek N, Muller WH, Arentshorst M, van der Mei HC, Ram AF, Dijksterhuis J, Wösten HAB**. 2013. Heterogeneity in liquid shaken cultures of *Aspergillus niger* inoculated with melanised conidia or conidia of pigmentation mutants. Stud Mycol **74:**47–57. http://dx.doi.org/10.3114/sim0008.
33. **Bleichrodt R**. 2012. Intercompartmental streaming in *Aspergillus*. Ph.D. thesis. University of Utrecht, Utrecht, The Netherlands.
34. **Masai K, Maruyama J, Sakamoto K, Nakajima H, Akita O, Kitamoto K**. 2006. Square-plate culture method allows detection of differential gene expression and screening of novel, region-specific genes in *Aspergillus oryzae*. Appl Microbiol Biotechnol **71:**881–891. http://dx.doi.org/10.1007/s00253-006-0429-z.
35. **Levin AM, de Vries RP, Conesa A, de Bekker C, Talon M, Menke HH, van Peij NN, Wösten HAB**. 2007. Spatial differentiation in the vegetative mycelium of *Aspergillus niger*. Eukaryot Cell **6:**2311–2322. http://dx.doi.org/10.1128/EC.00244-07.
36. **Levin AM, de Vries RP, Wösten HAB**. 2007. Localization of protein secretion in fungal colonies using a novel culturing technique; the ring-plate system. J Microbiol Methods **69:**399–401. http://dx.doi.org/10.1016/j.mimet.2007.01.003.
37. **Kasuga T, Glass NL**. 2008. Dissecting colony development of *Neurospora crassa* using mRNA profiling and comparative genomics approaches. Eukaryot Cell **7:**1549–1564. http://dx.doi.org/10.1128/EC.00195-08.
38. **Krijgsheld P, Altelaar AF, Post H, Ringrose JH, Müller WH, Heck AJ, Wösten HAB**. 2012. Spatially resolving the secretome within the mycelium of the cell factory *Aspergillus niger*. J Proteome Res **11:**2807–2818. http://dx.doi.org/10.1021/pr201157b.
39. **Krijgsheld P, Nitsche BM, Post H, Levin AM, Müller WH, Heck AJ, Ram AF, Altelaar AF, Wösten HA**. 2013. Deletion of *flbA* results in increased secretome complexity and reduced secretion heterogeneity in colonies of *Aspergillus niger*. J Proteome Res **12:**1808–1819. http://dx.doi.org/10.1021/pr301154w.
40. **Teertstra WR, Lugones LG, Wösten HAB**. 2004. In situ hybridisation in filamentous fungi using peptide nucleic acid probes. Fungal Genet Biol **41:**1099–1103. http://dx.doi.org/10.1016/j.fgb.2004.08.010.
41. **Abadeh A, Lew RR**. 2013. Mass flow and velocity profiles in *Neurospora* hyphae: partial plug flow dominates intra-hyphal transport. Microbiology **159:**2386–2394. http://dx.doi.org/10.1099/mic.0.071191-0.
42. **Ramos-García SL, Roberson RW, Freitag M, Bartnicki-García S, Mouriño-Pérez RR**. 2009. Cytoplasmic bulk flow propels nuclei in mature hyphae of *Neurospora crassa*. Eukaryot Cell **8:**1880–1890. http://dx.doi.org/10.1128/EC.00062-09.
43. **Steinberg G**. 2007. Hyphal growth: a tale of motors, lipids, and the Spitzenkörper. Eukaryot Cell **6:**351–360. http://dx.doi.org/10.1128/EC.00381-06.
44. **Momany M, Richardson EA, Van Sickle C, Jedd G**. 2002. Mapping Woronin body position in *Aspergillus nidulans*. Mycologia **94:**260–266. http://dx.doi.org/10.2307/3761802.
45. **Lai J, Koh CH, Tjota M, Pieuchot L, Raman V, Chandrababu KB, Yang D, Wong L, Jedd G**. 2012. Intrinsically disordered proteins aggregate at fungal cell-to-cell channels and regulate intercellular connectivity. Proc Natl Acad Sci U S A **109:**15781–15786. http://dx.doi.org/10.1073/pnas.1207467109.
46. **Shen KF, Osmani AH, Govindaraghavan M, Osmani SA**. 2014. Mitotic

regulation of fungal cell-to-cell connectivity through septal pores involves the NIMA kinase. Mol Biol Cell **25:**763–775. http://dx.doi.org/10.1091/mbc.E13-12-0718.

47. **Safranyos RG, Caveney S.** 1985. Rates of diffusion of fluorescent molecules via cell-to-cell membrane channels in a developing tissue. J Cell Biol **100:**736–747. http://dx.doi.org/10.1083/jcb.100.3.736.
48. **Contreras JE, Sánchez HA, Véliz LP, Bukauskas FF, Bennett MV, Sáez JC.** 2004. Role of connexin-based gap junction channels and hemichannels in ischemia-induced cell death in nervous tissue. Brain Res Brain Res Rev **47:**290–303. http://dx.doi.org/10.1016/j.brainresrev.2004.08.002.
49. **Ehlers K, Kollmann R.** 2001. Primary and secondary plasmodesmata: structure, origin, and functioning. Protoplasma **216:**–1–30.